Finite element analysis on the capacity of circular concrete-filled double-skin steel tubular (CFDST) stub columns

M. Pagoulatou, T. Sheehan, X.H. Dai, D. Lam*

School of Engineering, University of Bradford, Bradford, UK

Abstract

This paper presents the behaviour of circular concrete-filled double-skin steel tubular (CFDST) stub columns compressed under concentric axial loads. To predict the performance of such columns, a finite element analysis is conducted. Herein, for the accurate modelling of the double-skin specimens, the identification of suitable material properties for both the concrete infill and steel tubes is crucial. The applied methodology is validated through comparisons of the results obtained from the finite element analysis with those from past experiments. Aiming to examine the effect of various diameter-to-thickness (D/t) ratios, concrete cube strengths and steel yield strengths on the overall behaviour and ultimate resistance of the double-skin columns, a total of twenty-five models are created to conduct the parametric study. In addition, four circular concrete-filled steel tubes (CFST) are included to check the dissimilarities, in terms of their behaviour and weight, when compared with identical double-skin tubes. A new formula based on Eurocode 4 is proposed to evaluate the strength of the double-skin specimens. Based on the comparison between the results derived from the analysis, the proposed formulae for the concrete filled double-skin would appear to be satisfactory.

1. Introduction

Concrete-filled double-skin steel tubes consist of two concentric steel tubes, an outer and an inner, with concrete sandwiched between them and a void at their centre. The outer and inner tubes can either have the same or different cross-sections, e.g. circular-circular, circular-square etc. Having recently been introduced for construction purposes, double-skin columns belong to the family of composite columns and therefore combine the best qualities of both steel and

*Corresponding author. Tel.: +441274234052; fax: +441274234525. E-mail address: d.lam1@bradford.ac.uk (D. Lam)

concrete. These columns are said to have similar behaviour to the single-skin columns, but with a lesser weight and greater stiffness.

Researchers in recent years have carried out experiments and finite element analyses to investigate the behaviour of concrete-filled double-skin stub members tested against compressive forces. Huang et al. [1] created fourteen specimens identical to those initially introduced by Tao et al [2] and Lin and Tsai [3], aiming to investigate the accuracy of modelling in ABAQUS. From the analysis of the stress-strain curves it was concluded that sections with a greater confinement factor (ξ) demonstrated strain-hardening behaviour, whilst strain-softening behaviour was shown for smaller ξ values. Yu et al. [4] focused on the parameters that affect the performance of concrete within a new kind of hybrid double-skin column. A new and simple stress-strain model was suggested for concrete in this type of cross-section. Elchalakani *et al*. [5] tested eight specimens with circular outer and square inner skins and Zhao *et al.* [6] tested six specimens with circular outer and inner skins. From the results, it was found that the buckling of both the outer and inner tubes were due to the failure of concrete. In addition, sections with large slenderness values appeared to be more ductile than those with small slenderness values. Similar tests were conducted by Tao *et al.* [2] who examined fourteen stub columns having both outer and inner circular hollow sections. The primary aspects under consideration in this study were the diameter-to-thickness ratio (D/t) and the hollow section ratio (a parameter relating the diameter of the inner hollow tube to the diameter of the outer tube). The analysis proved that the failure mode of the inner tube highly depends upon its D/t ratio, as opposed to that of the outer tube which was the same for various D/t ratios. Furthermore, the double-skin specimens did not appear to be influenced by the hollow section ratio. Polymer concrete sandwiched between the concentric tubes was studied by Wei *et al*. [7, 8]. The stability, strength and ductility of twenty-six columns were inspected. It was noticed that polymer concrete has an equivalent behaviour to the commonly used concrete, since it was the fracture of this component that allowed buckling of

the tubes to begin. A formula by which the strength of these members could be calculated was recommended and found to be accurate. Zhao *et al.* [9] performed tests on a series of short columns subjected to static and cyclic loads. It seemed that the latter loading condition can significantly influence the load-deformation curve, especially for specimens with large diameter to thickness ratios. Hu and Su [10] recommended three equations in order to best evaluate the lateral confining pressure f_1 and one design specification for the material degradation parameter k_3, which are needed for the modelling of the confined concrete in ABAQUS. Out of the three obtained values, the minimum value of f_1 was found to be the most suitable to be adopted for engineering purposes. Research by Uenaka *et al*. [11] based on twelve specimens observed that as D_i/D_o was increased, the performance of the double-skin columns reduced. It was noted that tensile stresses occurred in the outer tube, whereas compressive stresses occurred in the inner tube. The load bearing capacity of the specimens was found to be considerably influenced by the degree of confinement offered by the outer tube. The thermal as well as structural response of double-skin columns was investigated by Lu *et al.* [12], who simulated sixteen stub specimens in ABAQUS. The typical performance of a double-skin specimen included the outward and inward buckling of the outer and inner tube, respectively. After the analysis, it was concluded that the yield strength of the tubes, the length of the column and the perimeter of the outer tube were some of the most important constraints affecting the resistance of such members against fire. Experiments under long-term and short-term compressive loads were carried out by Han *et al.* [13]. In the long-term test, the strain of the columns increased rapidly during the early stages of the test and stabilized later. The ultimate strength, on the other hand, decreased under the maintained loads. Yang *et al.* [14] reported the behaviour of partially loaded double-skin specimens. Following the investigation, the results clarified that the bigger the hollow area at the centre of the column the less concrete required to fill the empty space between the two steel tubes, and the weaker the confinement of concrete.

This study aims to examine the overall behaviour of double-skin specimens tested under axial compressive forces. In order to achieve this, finite-element models were generated in ABAQUS paying particular attention to identifying appropriate stress-strain relationships for the materials. Past experimental tests on double-skin columns conducted by Tao *et al.* [2] and Zhao *et al.* [6] were utilized to verify the adopted methodology. An extensive parametric study was carried out, where the parameters investigated were the outer diameter-to-thickness (D_o/t_o) ratio, the inner diameter-to-thickness (D_i/t_i) ratio, the cube strength of the concrete infill (f_{cc}) and the yield strength of both steel tubes (f_{yo}, f_{yi}). A comparison between identical double-skin and single-skin concrete-filled tubes was also made in terms of their behaviour and weight. Eurocode 4 was used to calculate the strengths of the modelled specimens. A new formula was suggested, owing to the fact that the current European Codes do not yet include a verified equation to evaluate the capacity of the double-skin columns. It was concluded that the outcomes derived from the new equation were in good agreement with the results attained from ABAQUS.

Nomenclature

A_{ai}	The cross-sectional area of the inner steel tube
A_{ao}	The cross-sectional area of the outer steel tube
A_c	The cross-sectional area of the concrete
D	The diameter of a single-skin concrete-filled tube (CFST)
D/t	Diameter to thickness ratio of a single-skin concrete-filled tube (CFST)
D_o/t_o	Outer diameter to outer thickness ratio of a double-skin concrete-filled tube (CFDST)
D_i/t_i	Inner diameter to inner thickness ratio of a double-skin concrete-filled tube (CFDST)
D_i	The inner diameter of a double-skin concrete-filled tube (CFDST)
D_o	The outer diameter of a double-skin concrete-filled tube (CFDST)
E_{cc}	Modulus of elasticity of confined concrete
E_s	Modulus of elasticity of steel
$E_s(T)$	Modulus of elasticity of steel under a particular temperature
$E_1(T)$	Modulus of elasticity of steel multiplied by 0.01
f	Stress values
f_c, f_{cyl}	The unconfined concrete cylinder compressive strength (=0.8 x cube strength)

f_{cc}	The confined concrete compressive strength
f_{ck}	Characteristic strength of concrete
$f_{sy}(T)$	The yielding strength of the steel after exposure to high temperature (T)
f_{yi}	The yield strength of the inner steel tube
f_{yo}	The yield strength of the outer steel tube
f_1	The lateral confining pressure imposed by the circular steel tube
k_1, k_2	Enhancement factors of concrete taken as 4.1 and 20.5, respectively
k_3	The material degradation parameter
L	The length/height of the column
n_a	The reduction coefficient of the steel tube
n_{ai}	The reduction coefficient of the inner steel tube
n_{ao}	The reduction coefficient of the outer steel tube
n_c	The enhancement coefficient of concrete
n_{ci}	The enhancement coefficient of concrete from inner steel tube
n_{co}	The enhancement coefficient of concrete from outer steel tube
N_{FE}	The ultimate strength derived from the FE analysis
N_u	The ultimate strength calculated by Eurocode 4
$P_{analysis}$	The maximum load capacity of a specimen attained from the finite element analysis
P_{test}	The maximum load capacity of a specimen attained from the experimental tests
r	Reduction factor that takes into account the effect of concrete strength
R	Parameter dependent upon R_E and two equivalent constraints $R\sigma$ and $R\varepsilon$ and is equal to 4
R_E	Parameter related to the modulus of elasticity of concrete and the ratio of the confined strain ε_{cc} to the corresponding compressive strength f_{cc}
R_ε	Parameter in defining the stress-strain relationship of confined concrete
$R\sigma$	Parameter in defining the stress-strain relationship of confined concrete
t	The thickness of a single-skin concrete-filled tube (CFST)
T	Temperature to which concrete-filled tube is exposed
t_i	The thickness of the inner tube of a double-skin concrete-filled tube
t_o	The thickness of the outer tube of a double-skin concrete-filled tube
ε	Strain values
ε_c	The unconfined strain corresponding to fc
ε_{cc}	The confined strain corresponding to fcc
ε_{sy}	The strain corresponding to the fsy(T) value
ξ	Confinement factor for concrete-filled tube
σ_i	Stress in steel exposed to high temperatures

2. Finite element modelling

2.1 General information

For the simulation of circular concrete-filled double-skin steel tubes and the analysis of their behaviour, the finite element programme ABAQUS [15] was used. The aim is to create models that would accurately predict the behaviour of this form of composite columns, therefore the materials with their characteristic stress-strain curves needed to be defined separately along with their interactions, the loading and boundary conditions of each section as a unit, and the most suitable mesh selected.

2.2 Concrete

To begin with, the outer and inner tubes of concrete-filled double-skin composite columns restrain the sandwiched concrete, which therefore can be approached as confined. Fig. 1 depicts the stress-strain curve of the confined concrete, which is adopted, as well as that of the unconfined concrete. Eqs. (1) and (2) suggested by Mander et al. [16] for the confined stress and strain, symbolized as f_{cc} and ε_{cc} respectively, which originally referred to concrete-filled steel tubes can be applied:

$$f_{cc} = f_c + k_1 f_1 \ \text{(MPa)} \qquad (1)$$

$$\varepsilon_{cc} = \varepsilon_c \left(1 + k_2 \frac{f_l}{f_c} \right) \qquad (2)$$

where k_1 and k_2 are fixed constraints equal to 4.1 and 20.5, accordingly, as recommended in the study of Richart *et al*. [17]. Additionally, the term f_c stands for the unconfined cylinder strength of concrete, which is the equivalent of 0.8 times its cube strength, whereas ε_c represents the corresponding unconfined strain, which herein is set as 0.003. The remaining factor, f_c, introduces the dual lateral confining pressure that concrete undergoes, caused by the steel tubes.

Hu and Su [10] have recently proposed three new estimations, Eqs. (3) to (5), in order to calculate the value of the pressure, with respect to the influence of both tubes, as follows:

$$f_1 = 8.525 - 0.166 \left(\frac{D_o}{t_o}\right) - 0.00897 \left(\frac{D_i}{t_i}\right) + 0.00125 \left(\frac{D_o}{t_o}\right)^2 + 0.00246 \left(\frac{D_o}{t_o}\right) \times \left(\frac{D_i}{t_i}\right) - 0.00550 \left(\frac{D_i}{t_i}\right)^2 \geq 0 \quad (3)$$

$$\frac{f_l}{f_{yi}} = 0.01844 - 0.00055 \left(\frac{D_o}{t_o}\right) - 0.00040 \left(\frac{D_i}{t_i}\right) + 0.00001 \left(\frac{D_o}{t_o}\right)^2 + 0.00001 \left(\frac{D_o}{t_o}\right) \times \left(\frac{D_i}{t_i}\right) - 0.00002 \left(\frac{D_i}{t_i}\right)^2 \quad (4)$$

$$\frac{f_l}{f_{yo}} = 0.01791 - 0.00036 \left(\frac{D_o}{t_o}\right) - 0.00013 \left(\frac{D_i}{t_i}\right) + 0.00001 \left(\frac{D_o}{t_o}\right)^2 + 0.00001 \left(\frac{D_o}{t_o}\right) \times \left(\frac{D_i}{t_i}\right) - 0.00002 \left(\frac{D_i}{t_i}\right)^2 \quad (5)$$

in which D_o is the diameter of the outer tube and t_o is its thickness, while D_i is the diameter of the inner steel tube and t_i is its thickness. Similarly, f_{yi} and f_{yo} are the yield strengths of the inner and outer tube, respectively.

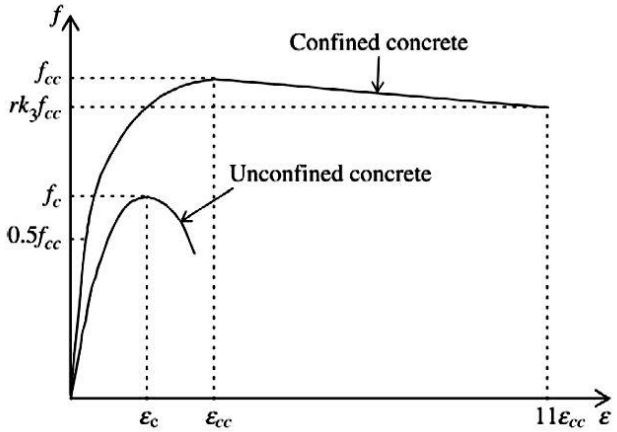

Fig. 1. Stress-strain curves for both confined and unconfined concrete

To predict the nonlinear behaviour of concrete the following formula, Eq. (6), proposed by Saenz [18] is employed:

$$f = \frac{E_{cc}\,\varepsilon}{1+(R+R_E-2)\left(\frac{\varepsilon}{\varepsilon_{cc}}\right)-(2R-1)\left(\frac{\varepsilon}{\varepsilon_{cc}}\right)^2+R\left(\frac{\varepsilon}{\varepsilon_{cc}}\right)^3}\ \text{(MPa)} \qquad (6)$$

where the modulus of elasticity E_{cc} is given by ACI [19], R and R_E can be expressed via the subsequent formulas, Eqs. (7) to (9):

$$E_{cc} = 4700\sqrt{f_{cc}}\ \text{(MPa)} \qquad (7)$$

$$R_E = \frac{E_{cc}\ \varepsilon_{cc}}{f_{cc}} \qquad (8)$$

$$R = \frac{R_E\,(R_\sigma - 1)}{(R_\varepsilon - 1)^2} - \frac{1}{R_\varepsilon} \qquad (9)$$

with R_σ and R_ε being both equal to 4, according to Hu and Schnobrich [20]. In this study, Poisson's ratio, ν_{cc} is defined as 0.2.

In order to estimate the last point of the descending region in the concrete stress-strain curve, the expression rk_3f_{cc} was used. This term considers the final stress value prior to failure and corresponds to a strain value of about $11\varepsilon_{cc}$. Constituting a coefficient for the degradation of confined concrete, directly related to the diameter-to-thickness ratio of both tubes, Eq. (10) is recommended by Hu and Su [10] to calculate k_3 as follows:

$$k_3 = 1.73916 - 0.00862\left(\frac{D_o}{t_o}\right) - 0.04731\left(\frac{D_i}{t_i}\right) - 0.00036\left(\frac{D_o}{t_o}\right)^2 + 0.00134\left(\frac{D_o}{t_o}\right)\left(\frac{D_i}{t_i}\right)$$

$$- 0.00058\left(\frac{D_i}{t_i}\right)^2 \geq 0 \qquad (10)$$

In this study, the above formula is assumed to be valid only when accompanied by the reduction factor r, which can be accepted as unity for concrete cube strengths up to 30 MPa, validated by Giakoumelis and Lam [21], or as 0.5 for concrete cube strengths greater or equal to 100 MPa, in

line with Tomii [22] and; Mursi and Uy [23]. For the identification of r for all the strengths in between, linear interpolation is exercised.

Concrete in ABAQUS is treated as an elastic material until the confined strength f_{cc} is reached and then as plastic through the Drucker Prager option. This selection enables the comprisal of the angle of friction together with the flow stress ratio at values of 20 degrees and 0.8, respectively. The stress-strain values obtained for the plastic area, from Eq. (6), are then inserted in the Drucker Prager Hardening sub-option in the programme.

2.3 Steel

The typical stress-strain curve, considered for the precise simulation of steel's behaviour, consists of two zones as suggested by Han and Huo [24] and shown in Fig. 2. The linear elastic and nonlinear plastic sections of the curve can be attained easily by the Eqs. (11) and (12), respectively:

$$\sigma_i = E_s (T) \times \varepsilon \quad \text{for } \varepsilon \leq \varepsilon_{sy} (T) \tag{11}$$

$$\sigma_i = f_{sy} (T) + E_1 (T) \times [\varepsilon - \varepsilon_{sy} (T)] \quad \text{for } \varepsilon > \varepsilon_{sy} (T) \tag{12}$$

where $f_{sy}(T)$ is the yield strength of steel after fire exposure to a given temperature T and $\varepsilon_{sy}(T)$ is the corresponding strain expressed by Eq. (13) as follows:

$$\varepsilon_{sy} (T) = \frac{f_{sy} (T)}{E_s (T)} \tag{13}$$

Herein, given that the experiments are performed at normal room temperature, the temperature T in the above expressions does not influence the stresses or strains of the steel tubes. The initial

modulus of elasticity $E_s(T)$, taken as 200,000 N/mm^2, is required for the estimation of the $E_1(T)$ factor which is equivalent to 0.01 x $E_s(T)$. Poisson's ratio for the steel is set to be 0.3.

Steel in ABAQUS is treated as elastic up to its yield strength and as plastic from that point to the final strain under consideration, about 3%.

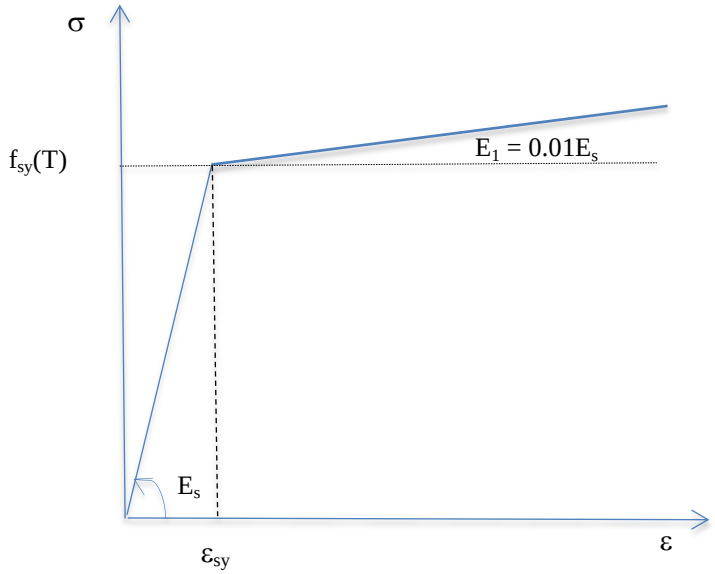

Fig. 2. Stress-strain curve for both outer and inner steel tubes

2.4 Interactions and surfaces

To achieve an equal shortening of the entire section, end plates were included in the model. Five individual components were used in total for each specimen: the outer and inner tubes, the concrete infill and the top and bottom endplates. The interactions between these components were defined by using surfaces, where one surface acted as the master surface and the other as the slave surface. The difference between a master and a slave surface is that the former can penetrate the latter, but the reverse can not take place. The steel tubes were chosen to be the master surfaces during their interaction with the concrete, but were treated as slave surfaces when in contact with the endplates. The concrete was also the slave surface during its interaction with both endplates. Eight pairs of surfaces were created for each double-skin specimen. In ABAQUS, the term "normal behaviour" refers to the pressure developed between the surfaces of

each pair whereas the term "tangential behaviour" describes the extent of friction and the occurrence of slippage between the two surfaces, caused by high shear stresses. Herein, the 'hard contact' was selected to represent the normal behaviour, while the 'rough' friction was used for the plate-concrete and plate-steel interactions and the 'penalty' friction for the core-tube interaction with a coefficient of friction equal to 0.3.

Table 1 Dimensions and material properties of circular concrete-filled double-skin steel tubes used for the verification study

Ref.	Dimensions							Material properties			Tested by
	D_o (mm)	t_o (mm)	D_o/t_o	D_i (mm)	t_i (mm)	D_i/t_i	L (mm)	f_c (MPa)	f_{yo} (N/mm^2)	f_{yi} (N/mm^2)	
cc2a	180	3	60	48	3	16	540	47.4	275.9	396.1	Tao et al. [2]
cc3a	180	3	60	88	3	29.33	540	47.4	275.9	370.2	
cc6a	240	3	80	114	3	38	720	47.4	275.9	294.5	
C1C7	114.5	5.9	19.41	48.4	2.8	17.29	400	63.4	454	425	Zhao et al. [6]
C2C7	114.6	4.7	24.38	48.4	2.8	17.29	400	63.4	416	425	
C5C8	165.1	3.5	47.17	101.8	3.1	32.84	400	63.4	433	410	

2.5 Loading conditions

The loading conditions were applied using the boundary conditions of each cross-section. The bottom endplate was fixed against all degrees of freedom. On the other hand, the node in the centre of the top endplate was fixed against all types of rotation and against lateral displacements (x and y directions). The top plate for all specimens was able to deform along the longitudinal (z) axis, along which the compressive loads were to be applied. The load was applied by specifying a displacement at this end equivalent to one sixth of the columns' total length in the boundary conditions. The rest of the nodes on the top endplates and down the columns are free to rotate or displace in any direction. Fig. 3 shows the loading condition of the FE model.

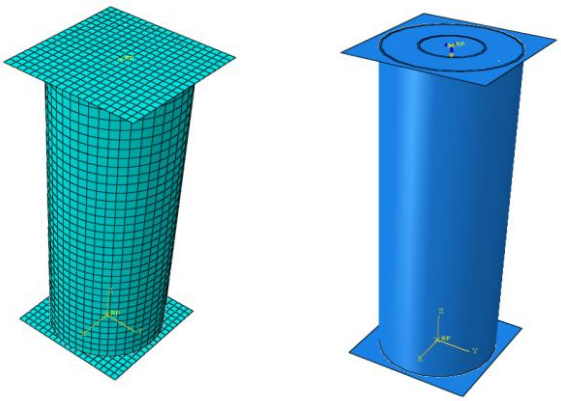

Fig. 3. Mesh and boundary conditions

2.6 Element mesh

All the parts composing the double-skin composite columns, apart from the endplates, were modelled with a similar mesh size. Occasionally, the concrete component needed slightly fewer elements than the steel tubes, and the inner steel tube needed fewer elements than the outer one. Generally, the average mesh size used was 25 mm for the concrete, 21 mm for the outer steel tube, 19 mm for the inner steel tube and 14 mm for both endplates. Fig. 4 shows the meshing arrangement of the CFDST columns

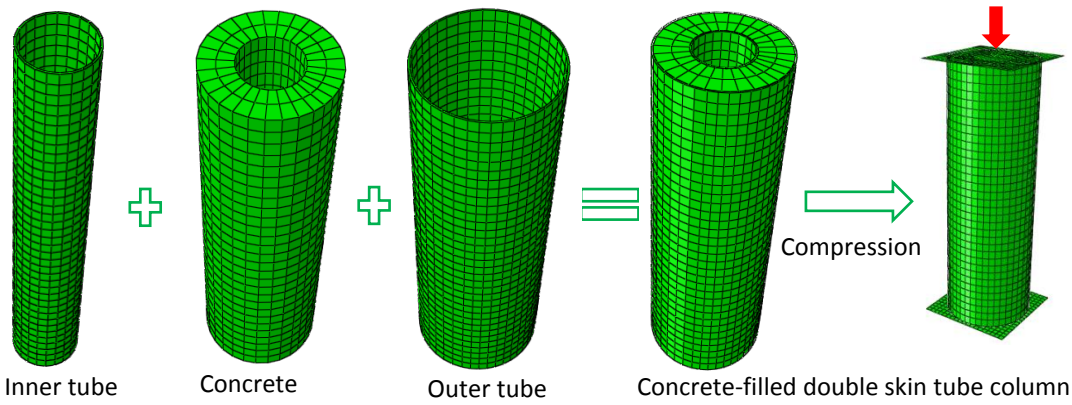

Fig. 4. Meshing of the CFDST columns

3. Verification study

3.1 Experimental results

To verify the methodology described in this study, past experiments conducted by other researchers on circular concrete-filled double-skin columns were selected and modelled in ABAQUS. A total of six specimens were adopted for this purpose, three from Tao et al. [2] and another three from Zhao *et al.* [6]. Table 1 summarises the dimensions and material properties of the chosen columns. As shown, specimens cc2a and cc3a shared the same outer tube diameter of 180 mm and thickness of 3 mm. Specimen cc6a had a bigger outer tube diameter of about 240 mm, but identical thickness to cc2a and cc3a. Therefore, the diameter-to-thickness ratio for the outer steel tubes (D_o/t_o) was 60 for the first two specimens and 80 for the third specimen. A wide range of diameters were used for the inner tubes. In particular, cc2a had a nominal inner diameter of 48 mm, cc3a of 88 mm and cc6a of 114 mm. With equal thicknesses of 3 mm, the diameter-to-thickness ratio for the inner steel tubes (D_i/t_i) varied between 16 mm and 38 mm. Moreover, two specimen lengths were tested by Tao et al. [2]: 540 mm and 720 mm. For the first three columns, the concrete infill used in all specimens had a cube strength of 47.4 MPa, while the outer steel tubes all had a yield strength of 275.9 N/mm^2. In contrast, the inner steel tubes were all of various strengths with cc2a having a yield capacity of 396.1 N/mm^2, cc3a of 370.2 N/mm^2 and cc6a of 294.5 N/mm^2.

The next three circular double-skin specimens under consideration, examined by Zhao *et al.* [6], had a nominal length of 400 mm. Two nominal diameters of 114.5 mm and 165.1 mm were used for the outer steel tubes, whereas three nominal thicknesses of 5.9 mm, 4.7 mm and 3.5 mm were employed. The outer diameter-to-thickness ratios (D_o/t_o) ranged from 19.41 to 47.17. Specimens C1C7 and C2C7 had similar inner tube dimensions, whilst specimen C5C8 was 101.8 mm wide and 3.1 mm thick. The inner diameter-to-thickness ratios (D_i/t_i) were 17.29 for the first two columns and 32.84 for the last column. The concrete cube strength of all the specimens derived

from this analysis was 63.4 MPa. The yield stresses of the outer steel tubes lay between 416 N/mm^2 and 454 N/mm^2, whereas that of the inner tubes had a smaller range of 410 N/mm^2 to 425 N/mm^2.

3.2 Comparison between the experimental and finite element analysis results

The comparison of the experimental observations with the modelled results was drawn using three parameters: the ultimate capacities, the axial load-strain curves and the final deformations of the specimens. Table 2 shows the recorded maximum strengths of the test specimens together with the attained ultimate resistances of the specimens modelled in ABAQUS. Good agreement was noted generally, with the tested-to-finite element model strength ratios being close to unity. According to the programme five out of six circular double-skin models were estimated to have performed better in ABAQUS than in the corresponding experiments. Nonetheless, the average value among the strengths ratios was 0.93.

Table 2 Comparison between the experimental and finite element capacities

Specimen	P_{test} (kN)	$P_{analysis}$ (kN)	$\frac{P_{test}}{P_{analysis}}$
cc2a	1790	1823.67	0.98
cc3a	1648	1609.83	1.02
cc6a	2421	2724.09	0.89
C1C7	1415	1686.39	0.84
C2C7	1380	1466.88	0.95
C5C8	1705	1905.51	0.89
Average value	-	-	0.93

The load-strain behaviour of the first three circular double-skin specimens, namely cc2a, cc3a and cc6a, was also observed. Fig. 5 exhibits the expected versus achieved curves of the last two columns, cc3a and cc6a. Specimen cc3a demonstrated the same post-peak behaviour and ultimate load. However, the numerical model exhibited superior ductility to its experimental

counterpart. Furthermore, specimen cc6a displayed an equal load-strain performance up to the point where the experimental column reached its maximum capacity. The model showed better behaviour both in terms of its ultimate strength and ductility. The load-strain behaviour of the second group of columns, that is C1C7, C2C7 and C5C8, was investigated in a similar way. Fig. 6 compares the experimental results from Zhao *et al.* [6] with those from the ABAQUS models for specimens C1C7 and C2C7. Specimen's C1C7 test and finite element model axial load-strain curve results followed a similar pattern, although the difference between the maximum strengths was as great as 200 kN. The finite element method was also significantly more ductile than the test member. The model of specimen C2C7 had similar loads to those of the test specimen, but there were differences in the corresponding strain values. Once again, the methodology used in this study to simulate the column increased its flexibility in comparison with the behaviour observed in the experiments.

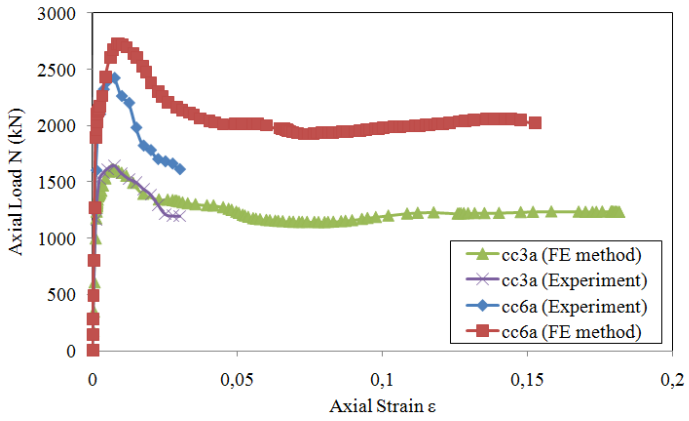

Fig. 5. Experimental versus analysed axial load-strain curves for specimens cc3a and cc6a.

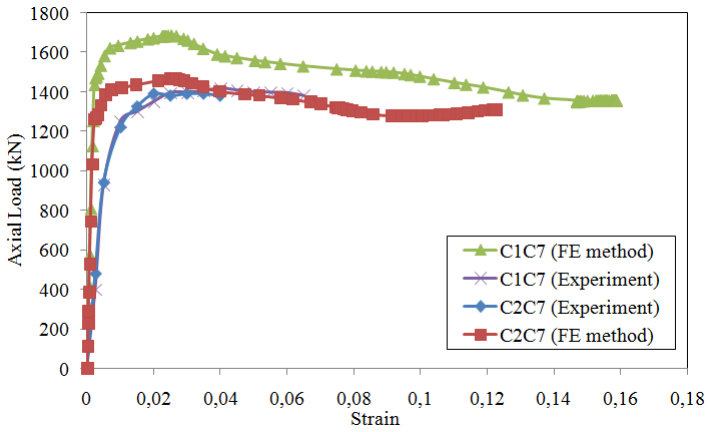

Fig. 6. Experimental versus analysed axial load-strain curves for specimens C1C7 and C2C7.

The final shapes of the tested columns were compared with those of the models to verify the level of this study's accuracy. Fig. 7 presents both these shapes for column cc3a prior to failure. It was found that the shortening of the specimen was close to reality. Specimens cc2a, cc3a and cc6a buckled mostly around the mid-height in the form of outward folds. Fig. 8 presents the failure shape of column C5C8, which displayed two outward folds, one near each end of the column.

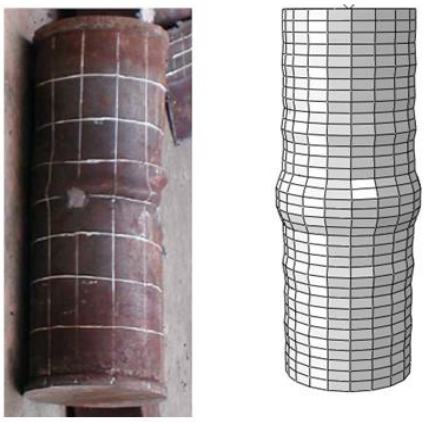

(a) Experimental (b) FE analysis

Fig. 7. Comparison of the experimental and analysed failure modes of specimen cc3a.

(a) Experimental (b) FE analysis

Fig. 8. Comparison of the experimental and analysed failure modes of specimen C5C8.

4. Parametric study

For this study, a total of 25 columns were considered to analyse the effect of the dimensions and material properties on the overall behaviour of the double-skin columns. Table 3 summarises the characteristics of the specimens adopted and modelled in ABAQUS. In order to distinguish between the investigated parameters, the columns were divided into six groups. The nominal length of all the specimens chosen under this parametric study was 400 mm. The first group, namely OS-D, consisted of four specimens having outer steel diameters ranging from 70 mm to 145 mm and a uniform thickness of 2.5 mm. The diameter-to-thickness ratio of these columns was between 28 and 58, covering the first three classes of tubular cross-section according to Eurocode 4 [25]. The second group, namely OS-T, comprised four specimens with the same outer diameter (D_o) set as 145 mm, but various outer tube thicknesses equal to 1.5 mm, 3.5 mm, 4.5 mm and 5.5 mm. The ratio D_o/t_o covered a greater range of values between 26.36 and 96.67. These two groups, OS-D and OS-T, had the exact same inner tube dimensions with a diameter of 58 mm and a thickness of 2.5 mm. Next, group IS-D examined the impact of the inner tube diameter variations and therefore the specimens considered under this collection had different diameters ranging from 60 mm to 125 mm. On the other hand, the IS-T group inspected the

effect of inner tube thickness on the column's capacity. As a result, a set of thicknesses between 1.5 mm and 5.5 mm was chosen. Both IS-D and IS-T groups shared the same outer tube dimensions with a diameter of 145 mm and a thickness of 2.5 mm. Additionally, a concrete cube strength of 60 MPa and steel yield strength, for both the outer and inner tubes, of 355 N/mm^2 were applied to all components in groups OS-D, OS-T, IS-D and IS-T.

The fifth group of specimens, named CF, contained four double-skin columns of normal and high-strength concrete, with strengths of 40, 80, 100 and 120 MPa. These columns had outer and inner tube diameters of 120 mm and 90 mm, respectively, outer and inner tube thicknesses of 2.5 mm, together with the same outer and inner steel tube strength of 355 N/mm^2. The last group of specimens, namely SS, focused on combinations of steel strengths for the tubes of each column. Outer-inner tube strengths of 275-275 N/mm^2, 355-420 N/mm^2, 275-460 N/mm^2, 420-355 N/mm^2 and 460-275 N/mm^2 were examined, whilst the dimensions and the concrete strength of all five columns in this group remained unaffected.

Table 3 Dimensions and material properties of circular concrete-filled double-skin steel tubes used for the parametric study

Group	Specimen	Dimensions							Material properties		
		D_o (mm)	t_o (mm)	D_o/t_o	D_i (mm)	t_i (mm)	D_i/t_i	L (mm)	f_c (MPa)	f_{yo} (N/mm^2)	f_{yi} (N/mm^2)
1 (OS-D)	OS-D1	70	2.5	28.00	58	2.5	23.20	400	60	355	355
	OS-D2	87.5	2.5	34.31	58	2.5	23.20	400	60	355	355
	OS-D3	112.5	2.5	45.00	58	2.5	23.20	400	60	355	355
	OS-D4	145	2.5	58.00	58	2.5	23.20	400	60	355	355
2 (OS-T)	OS-T1	145	1.5	96.67	58	2.5	23.20	400	60	355	355
	OS-T2	145	3.5	41.43	58	2.5	23.20	400	60	355	355
	OS-T3	145	4.5	32.22	58	2.5	23.20	400	60	355	355
	OS-T4	145	5.5	26.36	58	2.5	23.20	400	60	355	355
3 (IS-D)	IS-D1	145	2.5	58.00	60	2.5	24.00	400	60	355	355
	IS-D2	145	2.5	58.00	77	2.5	30.80	400	60	355	355
	IS-D3	145	2.5	58.00	105	2.5	42.00	400	60	355	355
	IS-D4	145	2.5	58.00	125	2.5	50.00	400	60	355	355
4 (IS-T)	IS-T1	145	2.5	58.00	110	1.5	73.33	400	60	355	355
	IS-T2	145	2.5	58.00	110	3.5	31.43	400	60	355	355
	IS-T3	145	2.5	58.00	110	4.5	24.44	400	60	355	355
	IS-T4	145	2.5	58.00	110	5.5	20.00	400	60	355	355
5 (CF)	CF1	120	2.5	48.00	90	2.5	36.00	400	40	355	355
	CF2	120	2.5	48.00	90	2.5	36.00	400	80	355	355
	CF3	120	2.5	48.00	90	2.5	36.00	400	100	355	355
	CF4	120	2.5	48.00	90	2.5	36.00	400	120	355	355
6 (SS)	SS1	175	4.5	38.89	130	3.5	37.14	400	60	275	275
	SS2	175	4.5	38.89	130	3.5	37.14	400	60	355	420

	SS3	175	4.5	38.89	130	3.5	37.14	400	60	275	460
	SS4	175	4.5	38.89	130	3.5	37.14	400	60	420	355
	SS5	175	4.5	38.89	130	3.5	37.14	400	60	460	275

4.1 Discussion

4.1.1 Strength

The ultimate resistance of the circular concrete-filled double-skin steel tubes obtained from ABAQUS was one of the main results of interest. Table 4 shows the strengths derived after the finite element analysis on the columns under investigation. Starting from the first group of columns, namely OS-D, where the parameter under investigation was the cross-sectional size of the outer steel tube, it became obvious that for a constantly increasing outer diameter the strength of the specimens was also steadily enhanced. From the second group of columns, i.e. OS-T, it was shown that the increment in the thickness of the outer tube benefited the capacity of the specimens; nonetheless the improvement noted was less significant than that offered by the increase in diameter. Similar to the first two groups, the IS-D and IS-T groups aimed to examine the influence of the cross-sectional size as well as thickness of the inner tube on the resistance of the members. It was concluded that as opposed to the enlargement of the outer diameter, specimens with wide inner diameter tubes demonstrated a reduction in terms of their maximum capacities. By maintaining the same outer steel tube diameter, the increase in size of the inner steel tube diameter results in decreasing the area of the concrete, which provides a vital contribution in resisting the compressive loads acting on the column. On the other hand, the increment in the thickness of the inner tube exhibited a similar behaviour to that of the outer tube. The fifth group, namely CF, which investigated various concrete strengths, indicated that the ultimate resistance of the columns appeared to rise with the increase in the load bearing capacity of the concrete infill. From the sixth group of columns, it can be seen that the members with higher outer than inner steel yield strengths, such as SS4 and SS5, outperformed the columns with the exact opposite steel strength properties, i.e. SS2 and SS3. This is probably due

to the fact that the outer tube has a larger cross-sectional size compared to the inner tube, which allows it to resist a higher load.

4.1.2 Axial load - Displacement curve

The axial load-displacement curves of all the double-skin specimens involved were plotted and discussed accordingly in groups. Figs. 9, 10 and 11 demonstrate the curves obtained from ABAQUS of groups 1 (OS-D), 3 (IS-D) and 6 (SS), respectively. It can be seen that as the outer diameter gets wider, the increment of the load bearing capacity of the specimens appears to get greater. Moreover, it was observed that big outer steel cross-sections enhanced the ductility of the specimens, whilst causing a more noticeable decrease in the capacity of the specimens after the maximum strength was attained. As opposed to the effect of wide outer steel cross-sections, wide inner steel cross-sections were proved to result in the reduction of the resistance of the double-skin columns. Specifically, it was noted that the smaller the inner steel tube diameter, the greater the capacity achieved. Better ductility levels were also maintained by the columns with small inner tube cross-sectional sizes. Nevertheless, it was these members that demonstrated the most considerable decrease in terms of their load bearing capacity after reaching the maximum load. Examining the curves of specimens with the same steel yield strength for both tubes, greater inner than outer steel yield strength and vice versa indicated a few interesting results. It became clear that when the same steel properties were applied to both skins, the capacity and ductility obtained were less than in any other case. Furthermore, the resistance of columns with more enhanced outer than inner steel tubes was found to be significantly greater when compared against specimens with stronger inner than outer steel tubes.

Table 4 Comparison of the analysis results with the calculated by the proposed formula outcomes

Group	Specimen	N_{FE} (kN)	N_u (kN) [Eq. 14]	N_u (kN) [Eq. 15]	N_u (kN) [Eq. 16]	N_{FE}/N_u [Eq.16]
1	OS-D1	398.70	368.42	380.72	350.61	1.14
	OS-D2	570.73	659.89	716.98	575.60	0.99
	OS-D3	856.15	1172.58	1343.43	955.74	0.90
	OS-D4	1336.27	2024.80	2398.38	1543.09	0.87
2	OS-T1	1389.01	1843.23	2198.53	1315.33	1.06
	OS-T2	1451.58	2197.75	2587.72	1760.45	0.83
	OS-T3	1609.63	2362.26	2766.80	1967.48	0.82
	OS-T4	1731.18	2518.55	2935.86	2164.31	0.80
3	IS-D1	1322.15	1985.04	2346.79	1531.56	0.86
	IS-D2	1200.57	1683.89	1957.62	1411.56	0.85
	IS-D3	1052.16	1230.06	1380.58	1126.36	0.93
	IS-D4	899.83	887.00	954.54	854.91	1.05
4	IS-T1	1029.17	978.76	1100.23	971.51	1.06
	IS-T2	1131.26	1314.76	1450.20	1154.68	0.98
	IS-T3	1291.38	1481.84	1621.58	1244.05	1.04
	IS-T4	1440.14	1647.98	1790.73	1331.86	1.08
5	CF1	696.80	837.57	906.36	740.14	0.94
	CF2	819.62	954.37	1061.90	899.61	0.91
	CF3	887.46	1014.12	1139.69	979.35	0.91
	CF4	949.93	1074.42	1217.54	1059.11	0.90
6	SS1	1454.74	1698.68	1902.74	1602.68	0.91
	SS2	1807.15	2201.90	2430.76	1986.99	0.91
	SS3	1669.16	2068.26	2291.60	1800.28	0.93
	SS4	1888.56	2244.53	2476.35	2103.18	0.90
	SS5	1892.50	2190.44	2421.44	2132.03	0.89
					S.D.	0.089
					Mean	0.938
					COV	0.095

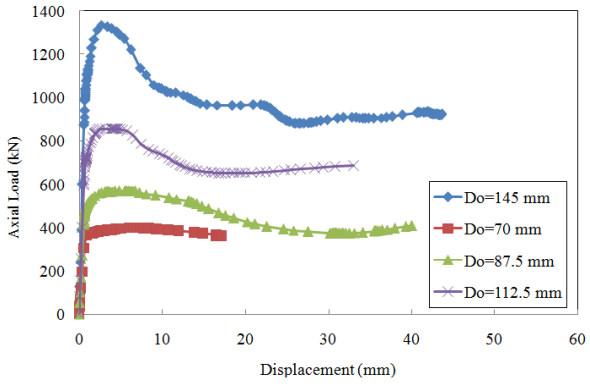

Fig. 9. Axial load-displacement curves for various outer tube diameters within group 1 (OS-D).

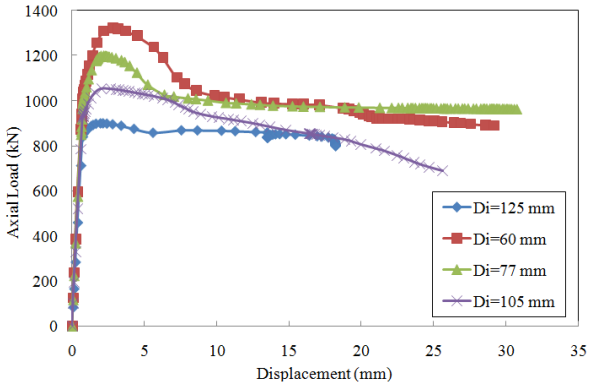

Fig. 10. Axial load-displacement curves for various inner tube diameters within group 3 (IS-D).

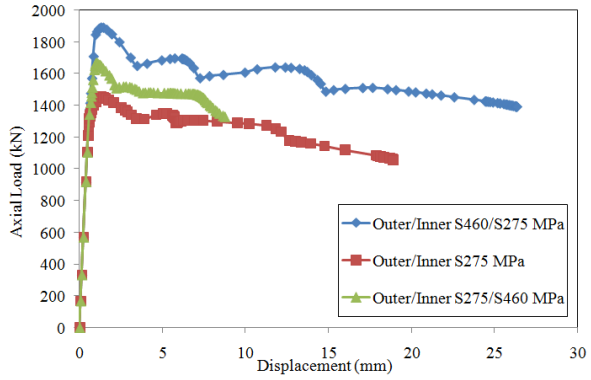

Fig. 11. Axial load-displacement curves for various outer and inner tube properties within group 6 (SS).

4.1.3 Failure mode

The final deformation of all the specimens under consideration was obtained from ABAQUS and Fig. 12 shows the shape of the concrete infill of the columns in the fifth group (see Table 3). All four specimens exhibited similar failure mode, experiencing two folds along the height of the column. The columns with the weakest concrete infill, i.e. 40 MPa demonstrated significant deformation than those with stronger infill. It is noticed that the spacing to the position of the folds along the column height would appear to be influenced by the concrete strength, the higher the concrete strength, the further apart between the folds. Figs. 13 and 14 exhibit the stresses undertaken by the outer and inner tubes of the SS2 and SS4 specimens. It can be noted that due to the reversed yield strengths adopted for the skins of these two columns, the stresses

experienced by the outer tube of SS2 specimen are the same as those suffered by the inner tube of SS4 specimen. The difference between the ultimate resistances of these two columns lies in their shortening behaviour. Examining the failure mode of these columns, it was obvious that the column with the stronger outer than inner steel strength, namely SS4, experienced greater deformation prior to failure than the column with the opposite steel properties. The SS2 column showed two main outward ripples and multiple folds along its outer and inner skin, respectively, whilst column SS4 demonstrated one main outward buckle near the bottom end on both of its skins. It would suggest the outer skin with higher steel strength controlled the failure mode shape of the inner skin with lower steel strength.

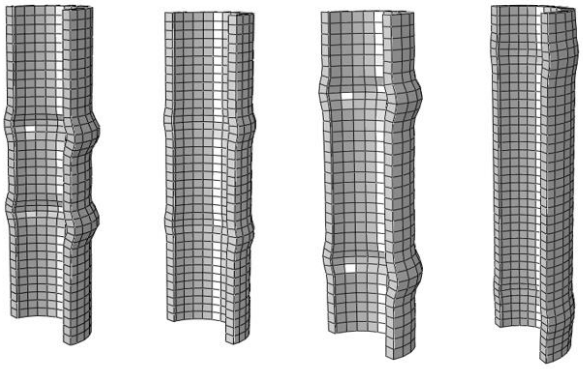

Fig. 12. From left to right the deformed shapes of the sandwiched concrete of the columns CF1, CF2, CF3 and CF4 within group 4 (CF).

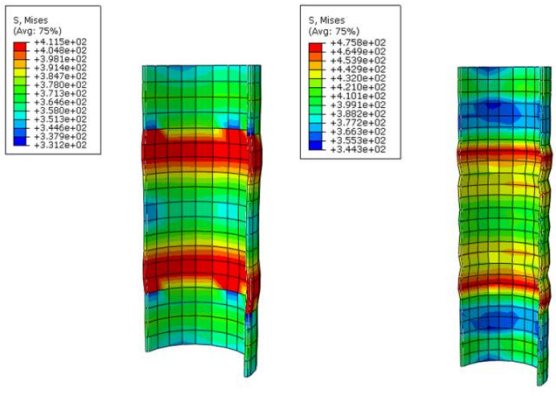

(a) Outer tube (b) Inner tube

Fig. 13. The stresses recorded on the outer and inner tube of specimen SS2.

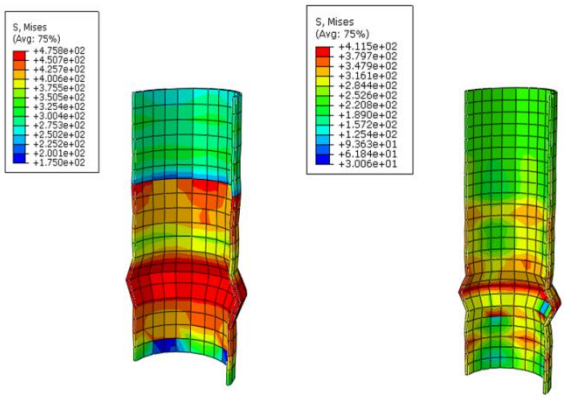

(a) Outer tube (b) Inner tube

Fig. 14. The stresses recorded on the outer and inner tube of specimen SS4.

4.2 Comparison between identical CFTs and CFDSTs

4.2.1 Behaviour

Aiming to further understand the concrete-filled double-skin tubular columns as well as the advantages that these columns offer, a comparison was made between some of the double-skin columns with their identical concrete-filled single-skin steel tubes. Initially four double-skin specimens were chosen from Table 4, namely OS-D1, CF2, OS-T1 and SS2, in order to then adopt four single-skin specimens of the same dimensions and properties. Table 5 summarises the concrete-filled single-skin steel tubes that were modelled in ABAQUS. Fig. 15 presents the axial load-displacement curves, of two single-skin columns together with their identical double-skin ones, which were obtained after the analysis was conducted. It can be inferred that generally the single-skin tubes behaved better in terms of both their capacity and ductility. This can be explained through the existence of concrete in the fully filled steel tubes and its increased participation into the loads carried by the columns. Table 6 contains the maximum capacities reached by the concrete-filled steel tubes.

Table 5 Capacities of single-skin CFST columns

Single-skin columns	
Specimen	Capacity (kN)
ST1	493.25
ST2	1057.80
ST3	2335.67
ST4	2160.99

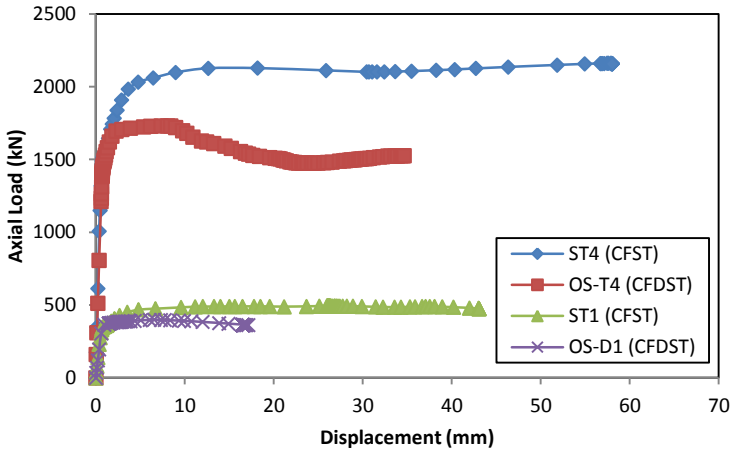

Fig. 15. Axial load-displacement comparison between identical single-skin and double-skin composite columns.

Table 6 Comparison of single-skin and double-skin columns capacities

Single-skin columns		Double-skin columns	
Specimen	Capacity (kN)	Specimen	Capacity (kN)
ST1	493.25	OS-D1	398.696
ST2	1057.80	CF2	819.621
ST3	2335.67	SS2	1807.150
ST4	2160.99	OS-T4	1609.630

4.2.2 Weight

A comparison was carried out between the weights of single-skin and double-skin concrete-filled members. With the purpose of estimating the weight of all the columns, the volume occupied by each material was calculated and assumptions were adopted for the individual material densities: the density of steel was taken as 79 kN/m³ while that of the concrete was taken as 24 kN/m³. Table 7 summarises the weights of the composite single-skin and double-skin columns. It can be

concluded that the concrete-filled double-skin steel tubes were lighter than their identical single-skin composite columns, mainly due to the quantity of concrete used.

Table 7 Weights comparison of the single-skin and double-skin columns

Single-skin columns		Double-skin columns		Weight reduction ratio (%)
Specimen	Weight (kg)	Specimen	Weight (kg)	
ST1	4.86	OS-D1	3.70	23.87
ST2	12.88	CF2	8.95	30.51
ST3	21.15	SS2	19.99	5.48
ST4	28.38	OS-T4	20.04	29.39

5. Eurocode 4

In this study, the approach of Eurocode 4 (EC4) was adopted to estimate the ultimate compressive strengths of the concrete-filled double-skin steel tubular columns. This standard currently accounts for the confinement effect of concrete by using a reduction factor n_a, for the contribution of the steel to the cross-section resistance and an enhancement factor n_c for the concrete contribution, both of which are determined using the non-dimensional global slenderness of the member and the eccentricity of applied loading. EC4 does not however consider the double-skin columns and therefore to overcome this issue the original equation proposed by EC4 for the single-skin columns was modified to take into account the effect of both steel tubes as well as the concrete enhancement of each member due to their existence, through separate enhancement (n_{co} and n_{ci}) and reduction (n_{ao} and n_{ai}) factors for each tube. The equation obtained was then as follows:

$$N_u = A_{ao}f_{yo}n_{ao} + A_{ai}f_{yi}n_{ai} + A_cf_c\left(1 + n_{co}\frac{t_o}{D_o}\frac{f_{yo}}{f_{cy1}} + n_{ci}\frac{t_i}{D_i}\frac{f_{yi}}{f_{cy1}}\right) \quad (14)$$

By comparing the analysis results with those predicted from the Eq. (14) it was observed that the formula significantly overestimated the strength of most of the specimens, apart from the OS-D1, IS-D4 and IS-T1 specimens. With the maximum deviation being as great as 34% a new formula was then proposed. The difference between this equation and the first one was that the former

only contained one confinement factor accounting for both steel tubes and another one for the concrete enhancement due to the tubes. The formula became as follows:

$$N_u = n_a(A_{ao}f_{yo} + A_{ai}f_{yi}) + A_c f_c\left(1 + n_c\left[\frac{t_o}{D_o}\frac{f_{yo}}{f_{cy1}} + \frac{t_i}{D_i}\frac{f_{yi}}{f_{cy1}}\right]\right) \quad (15)$$

This method was found to be even less reliable than the previous approach, as the deviation between the analysis and Eq. (15) results increased up to 44.3%. For that reason an additional approach was investigated. Assuming that the inner tube of these types of columns provides little enhancement to the sandwiched concrete, it was removed for the concrete's confinement factor. The final equation was given as:

$$N_u = n_a(A_{ao}f_{yo} + A_{ai}f_{yi}) + A_c f_c\left(1 + n_c\frac{t_o}{D_o}\frac{f_{yo}}{f_{cy1}}\right) \quad (16)$$

The calculated results from this formula are shown in Table 4. It can be seen that the ratio of the analysed over the predicted strengths of all the specimens under examination was close to unity. Looking at the first groups of columns it can be inferred that Eq. (16) was more precise for columns with small D_o/t_o ratio than for those with big D_o/t_o ratios. Additionally, it was noticed, from the fifth group of columns, that the strength of specimens filled with normal-strength concrete was evaluated with greater accuracy than the remaining specimens filled with high-strength concrete, this might due to the fact that current EC4 equation for column design is limited to normal strength concrete; i.e. up to C50/60 concrete. The formula also provided superior estimations for double-skin composite columns in which the outer tubes had lower yield strength values than the inner tubes, than for those in which the inner tubes had the weaker material. With a maximum deviation of 20%, it was concluded that the third equation achieved a good degree of accuracy in general.

6. Conclusions

A finite element analysis was conducted in order to examine the cross-sectional capacity and behaviour of the recently introduced composite double-skin columns subjected to concentric loading. Separate stress-strain curves were used for each of the materials in the model. Past experimental results were used to verify that the accuracy of the utilised method was sufficient. This was implemented by comparing the compressive resistance, axial load-strain curves and failure modes of the columns in the analysis to the test results obtained by the related researchers [2, 6]. When a good correlation was achieved between the test and analysis specimens, the same procedure was then employed for the parametric study. A total of twenty-five concrete-filled double-skin steel tubular columns and four concrete-filled steel tubular columns were adopted under this study and modelled in ABAQUS. The parameters investigated were the diameter of the outer and inner steel tube, the thickness of the outer and inner steel tube, the strength of the concrete used as an infill between the steel tubes, as well as the yield strength of both steel tubes. Comparisons between the behaviour and weight of both single-skin and double-skin composite columns were additionally performed. The capacities of the double-skin specimens were also evaluated using Eurocode 4. Owing to the fact that this code does not provide any specific rules related to double-skin columns, a new formula was proposed and verified against the analysis results. The proposed equation is valid for the determination of the ultimate compressive strength of the CFDST columns; it is generally found that the suggested equation is satisfactory.

References

[1] Huang H, Han LH, Tao Z, Zhao XL. Analytical behaviour of concrete-filled double skin steel tubular (CFDST) stub columns. Journal of Constructional Steel Research 2010; 66(9): 542-555.

[2] Tao Z, Han LH, Zhao XL. Behaviour of concrete-filled double skin (CHS inner and CHS outer) steel tubular stub columns and beam-columns. Journal of Constructional Steel Research 2004; 60(11): 1129-1158.

[3] Lin ML, Tsai KC. Behavior of double-skinned composite steel tubular columns subjected to combined axial and flexural loads. In: Proceedings of the first international conference on steel & composite structures. 2001. p. 1145-1152.

[4] Yu T, Teng JG, Wong YL. Stress-Strain Behavior of Concrete in Hybrid FRP-Concrete-Steel Double-Skin Tubular Columns. Journal of Structural Engineering 2010; 136(4): 379-389.

[5] Elchalakani M, Zhao XL, Grzebieta R. Tests on concrete filled double-skin (CHS outer and SHS inner) composite short columns under axial compression. Thin-Walled Structures 2002; 40(1): 415-441.

[6] Zhao XL, Grzebieta R, Elchalakani M. Tests on concrete filled double-skin CHS composite stub columns. Steel and Composite Structures 2002; 2(2): 129-146.

[7] Wei S, Mau ST, Vipulanandan C, Mantrala SK. Performance of New Sandwich Tube under Axial Loading: Experiment. Journal of Structural Engineering 1995; 121(12): 1806-1814.

[8] Wei S, Mau ST, Vipulanandan C, Mantrala SK. Performance of New Sandwich Tube under Axial Loading: Analysis. Journal of Structural Engineering 1995; 121(12): 1815-1821.

[9] Zhao XL, Tong LW, Wang XY. CFDST stub columns subjected to large deformation axial loading. Engineering Structures 2010; 32(3): 692-703.

[10] Hu HT, Su FC. Nonlinear analysis of short concrete-filled double-skin tube columns subjected to axial compressive forces. Marine Structures 2011; 24(5): 319-337.

[11] Uenaka K, Kitoh H, Sonoda K. Concrete filled double skin circular stub columns under compression. Thin-Walled Structures 2010; 48(8): 19-24.

[12] Lu H, Zhao XL, Han LH. FE modelling and fire resistance design of concrete filled double skin tubular columns. Journal of Constructional Steel Research 2011; 67(4): 1733-1748.

[13] Han LH, Li YJ, Liao FY. Concrete-filled double skin steel tubular (CFDST) columns subjected to long-term sustained loading. Thin-Walled Structures 2011; 49(8): 1534-1543.

[14] Yang YF, Han LH, Sun BH. Experimental behaviour of partially loaded concrete-filled double-skin steel tube (CFDST) sections. Journal of Constructional Steel Research 2012; 71(11): 63-73.

[15] ABAQUS. Analysis user's manuals and example problems manuals, version 6.9. Providence, Rhode Island: Abaqus, Inc.: 2009.

[16] Mander JB, Priestley MJN, Park R. Theoretical stress-strain model for confined concrete. Journal of Structural Engineering, ASCE 1988; 114(8): 1804-1826.

[17] Richart FE, Brandzaeg A, Brown RL. A study of the failure of concrete under combined compressive stresses. Bull. 185. Champaign (IL, USA): University of Illinois Engineering Experimental Station; 1928.

[18] Saenz LP. Discussion of 'Equation for the stress-strain curve of concrete' by P. Desayi, and S. Krishnan. Journal of the American Concrete Institute 1964;61:1229-1235.

[19] ACI. Building code requirements for structural concrete and commentary, ACI 318-399. Detroit (USA): American Concrete Institute; 1999.

[20] Hu HT, Schnobrich WC. Constitutive modeling of concrete by using nonassociated plasticity. Journal of Materials in Civil Engineering 1989;1(4):199-216.

[21] Giakoumelis G, Lam D. Axial capacity of circular concrete-filled tube columns. Journal of Constructional Steel Research 2004;60(7):1049-1068.

[22] Tomii M. Ductile and strong columns composed of steel tube, infilled concrete and longitudinal steel bars. In: Proc., 3rd int. Conf. On steel-concrete composite structures. Association of Steel-Concrete Structures, Fukuoka, Japan. 1991 [special volume]

[23] Mursi M, Uy B. Strength of concrete filled steel box columns incorporating interaction buckling. Journal of Structural Engineering, ASCE 2003;129(5):626-639.

[24] Han LH, Huo JS. Concrete-filled HSS columns after exposure to ISO-834 standard fire. Journal of Structural Engineering 2003; 129(1): 68-78.

[25] Eurocode 4, Design of composite steel and concrete structures. Part 1.1, General rules and rules for buildings, Incorporating corrigendum, BS EN1994-1-1, London (UK), British Standards Institution, 2009.